Coexistence of multiphase superconductivity and ferromagnetism in lithiated iron selenide hydroxide [(Li_{1−x}Fe_{x})OH]FeSe

Christian Urban, Ilya Valmianski, Ursula Pachmayr, Ali C. Basaran, Dirk Johrendt, and Ivan K. Schuller

Phys. Rev. B **97**, 024516 — Published 25 January 2018

DOI: 10.1103/PhysRevB.97.024516

Coexistence of multiphase superconductivity and ferromagnetism in lithiated iron selenide hydroxide $[(Li_{1-x}Fe_x)OH]FeSe$

Christian Urban[1], Ilya Valmianski[1], Ursula Pachmayr[2], Ali C. Basaran[1], Dirk Johrendt[2], Ivan K. Schuller[1]

[1] Department of Physics and Center for Advanced Nanoscience, University of California, San Diego, La Jolla, California 92093, USA

[2]Department of Chemistry, Ludwig-Maximilians-Universitaet Muenchen, D-81377, Munich, Germany

I. ABSTRACT

We present experimental evidence for a) multiphase superconductivity and b) coexistence of magnetism and superconductivity in a single structural phase of lithiated iron selenide hydroxide $[(Li_{1-x}Fe_x)OH]FeSe$ (LISH). Magnetic field modulated microwave spectroscopy (MFMMS) data confirms superconductivity with at least two distinct transition temperatures attributed to well defined superconducting phases at $T_{SC1} = 40\pm2$ K and $T_{SC2} = 35\pm2$ K. Magnetometry data for the upper critical fields reveals a change in the magnetic order ($T_M = 12$ K) below T_{SC1} and T_{SC2} that is consistent with ferromagnetism. This occurs because the superconducting coherence length is much smaller than the structural coherence length, allowing for several different electronic and magnetic states on a single crystallite. The results give new insight into the physics of complex multinary materials, where several phenomena governed by different characteristic length scales coexist.

II. INTRODUCTION

Understanding the coexistence of physical phenomena in multinary compounds is key for the development of functional materials. Some important classes of such materials are multiferroics,[1] magnetic superconductors,[2] as well as interfacially controlled[3,4] and proximity effect driven compounds.[5] In many cases, the systems being investigated are doped and are inhomogeneous on length scales shorter than the characteristic coherence length of the particular phenomena under study. Thus, it is important to understand how different length scales interact to give rise to an overall global response.[a]

A particularly interesting phenomenon is the coexistence of superconductivity (SC) and magnetism within the same compound. Examples include reentrant SC[6,7] where the SC competes directly with magnetism, SC with a high concentration of magnetic elements,[8] magnetic SC,[9,10] superlattices of FM and SC materials,[11-13] molecular magnetic SC[14,15] and FM-SC created by charge doping[14,16] or high pressure.[17] Very recently there have been claims of SC coexisting with FM at interfaces of insulating oxides.[4] For a recent review see reference 4 and 18.

Despite the many examples of materials that contain magnetic and SC elements, spatially coexisting SC and FM have been found in only a few systems and at very low temperatures. Significant efforts in the design of new materials by intercalating spacer layers into FeSe crystals lead to the discovery of the FM-SC, lithiated iron selenide hydroxide, $[(\mathrm{Li}_{0.8}\mathrm{Fe}_{0.2})\mathrm{OH}]\mathrm{FeSe}$ (LISH), with a record for FM-SC systems superconducting transition temperature (T_C) of 43 K.[19] The FM ordering temperature (10 K), is one of the highest and the SC volume fraction is very large, close to 100 % at 2 K, despite the long range magnetic order.

---

[a] *for a discussion of length scales see for instance Metallic Superlattices: The Study of Materials at Length Scales Ranging from a Few to Hundreds of Angstroms*[13]

The physical origin and nature of both transitions and its relation to each other in this class of Fe-based SC is still under debate.[19-26]

LISH is particularly well suited to address the interaction and length scales over which the structure, SC and magnetism interact. In order to study these we have used a combination of conventional structural and magnetic methods, together with magnetic field modulated microwave spectroscopy (MFMMS). MFMMS is a unique, highly sensitive, and selective technique[27] which provides information about inhomogeneous materials exhibiting multiple phase transitions.[28] Specifically, it has been extensively used to study SC systems[27,29,30] with multiple superconducting phases.[31] A unique advantage over other methods is its ability to distinguish phase transitions of different origins within the same compound.[28,29]

In this study, we present two main results. First, we find that crystallographically single phase polycrystalline samples of LISH exhibit multiple SC phases with distinct T_C's. Magnetometry data reveals that the SC coherence length is substantially shorter than the X-ray coherence length. Second, we show that these SC phases are coincidental with a new magnetic ordering appearing at $\boldsymbol{T_M = 12}$ K. This magnetic ordering is consistent with ferromagnetism.

III. EXPERIMENTAL

Polycrystalline $[(Li_{1-x}Fe_x)OH]FeSe$ (LISH) was synthesized under hydrothermal conditions analogous to reference with $x = 0.2$.[19] Briefly, Iron metal (99.9 %; 0.0851 g), Selenourea (99 %; 0.5 g) and $LiOH\cdot H_2O$ (3 g) were mixed with distilled water (10 mL), tightly sealed in a teflon-lined steel autoclave (50 mL) and heated at 155°C for 6 days. The shiny lamellar precipitates obtained were washed several times with distilled water, ethanol and dried under dynamic vacuum. The resulting compound is moderately temperature and air sensitive and needs to be stored at -25˚C under an inert (Ar) atmosphere. The transfer from the storage glass into the sample tubes for the MFMMS was done in an Ar glove box. The sample tube was then flushed 10 s with He gas before immediately being placed into the already cold measurement system (below -25˚C).

X-ray powder diffraction was carried out using a Huber G670 diffractometer with Cu-$K\alpha_1$ radiation (λ = 1.54 Å) and Ge-111 monochromator. Structural parameters were obtained from Rietveld refinement[32,33] of these diffraction data using the TOPAS software package.[34]

Magnetization measurements were performed using a Quantum Design DynaCool system equipped with a vibrating sample magnetometer (VSM) with a maximum field of 9 T and a temperature range between 1.8 and 400 K. The following protocol was used for the zero field cooling (ZFC) procedure: the samples were cooled to 2 K without applied field (H = 0 Oe). The magnetization was measured in a small field (typically 30 Oe) while heating the sample to 60 K, well above the $T_{c.}$ Subsequently the field cooling (FC) branch was obtained by cooling the sample to 2 K in the same small field. Hysteresis loops were recorded starting at zero field for different temperatures and the magnetization was measured as a function of increasing field up to the maximum field value. In between all measurements the magnet was oscillated around 0 Oe well above the sample T_c to minimize residual magnetic fields to less than 5 Oe.

A customized Bruker EleXsys X-band (9.4 GHz) Electron Paramagnetic Resonance (EPR) apparatus was used to perform MFMMS. The spectrometer was operated in a non-conventional mode in which the microwave absorption signal was measured as a function of temperature. A 100 KHz 15 Oe peak-to-peak modulation field was used to enhance the signal to noise. A small (15 Oe) external magnetic field was applied and kept constant during the measurement. As a result, the total applied magnetic field was always positive to avoid field dependent hysteretic effects. The sample was placed in the center of a rectangular dual mode cavity with microwave magnetic field is parallel to the modulation and external magnetic fields. The applied microwave power was chosen to be low enough (1 mW) to avoid sample heating. A flow cryostat was used to sweep the temperature from 300 K to 4 K at 5 K/min.

IV. RESULTS

Figure 1 shows the measured (blue) X-ray powder pattern together with an excellent (see Table I) refinement (red line) of a $[(Li_{1-x}Fe_x)OH]FeSe$ (LISH) single phase compound. The crystallographic data obtained are included in Table I. The numbers in between parenthesis are a Gaussian estimate of the error in the last significant figure. The tetragonal structure consists of *anti*-PbO type layers of lithium-iron-hydroxide alternating with FeSe layers in good agreement with literature values.[19-26] The R-values of the Rietveld refinement are exceptionally low (R_{wp} = 1.57, R_{exp}= 1.28) and, for example, significantly better than the R-values (R_{wp} = 7.35, R_{exp}= 4.71) in the determination of the now accepted structural model of YBCO.[35] The measured diffraction peaks arise from the superposition of instrumentally broadened peaks therefore the peak width provides a lower limit for the structural coherence length. Using the Scherrer formula, a structural coherence length of ξ_{XRD} = 91 nm is obtained from the average width of the diffraction peaks between 8 and 100° (2θ angle).

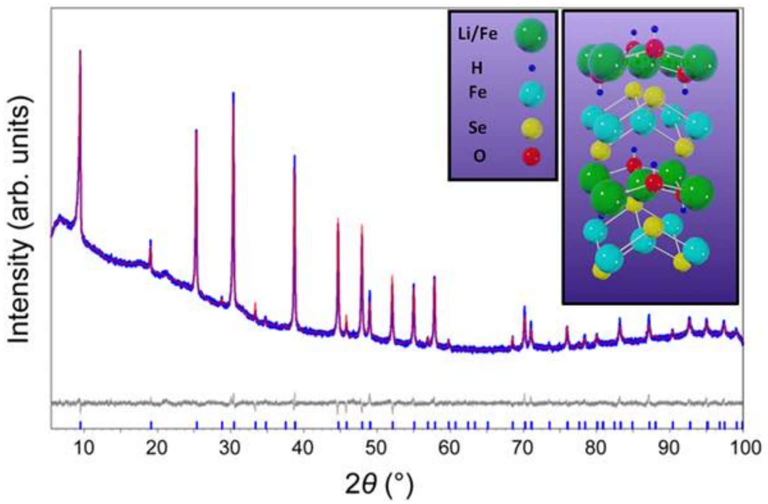

FIG. 1: X-ray powder diffraction (blue), Rietveld-refinement (red) and difference curve (gray) of $[(Li_{1-x}Fe_x)OH]FeSe$. The excellent agreement between experiment and refinement indicates a well-defined structurally homogeneous sample. The inset shows the structural model of the compound.

Table I. Crystallographic data of $[(Li_{1-x}Fe_x)OH]FeSe$.

$[(Li_{1-x}Fe_x)OH]FeSe$					
Crystal System	Tetragonal				
Space group	*P4/nmm* O1 (No. 129)				
a, *c* /pm	378.81(1), 927.14(4)				
V /nm^3	0.13304(1)				
R_{wp}, R_{exp}, χ^2	1.57, 1.28, 1.23				
Atomic positions					
Atom	*Wyck.*	*x*	*y*	*z*	occ.
Li1	2*a*	0	0	0	0.851(4)
Fe1	2*a*	0	0	0	0.149(4)
O	2*c*	0	1/2	0.0932(6)	1.0
H	2*c*	0	1/2	0.179(1)	1.0
Fe2	2*b*	0	0	1/2	1.0
Se	2*c*	1/2	0	0.3356(3)	1.0

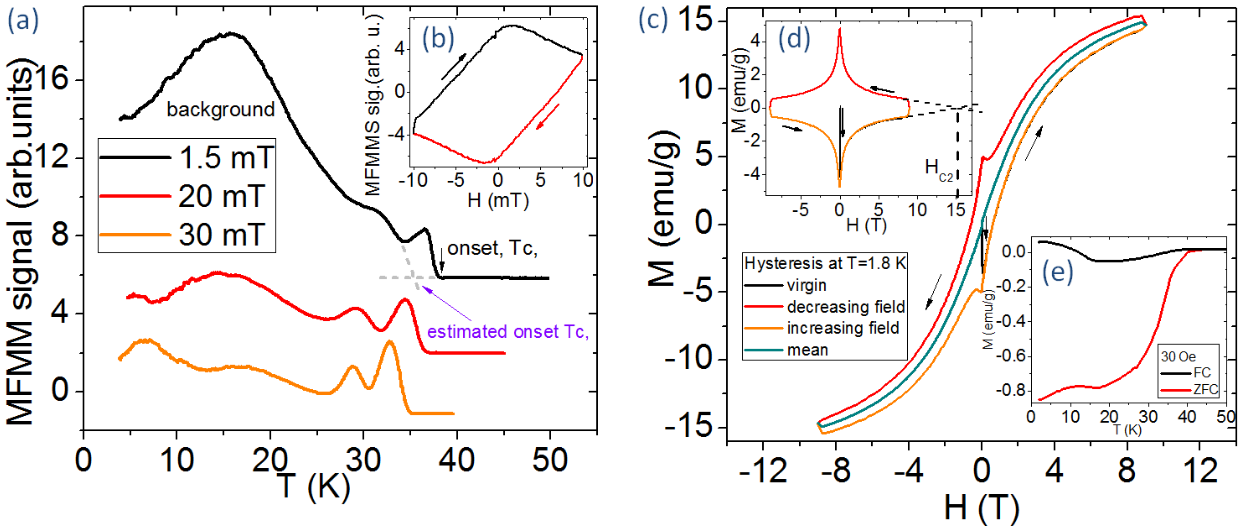

FIG. 2: (a) Magnetic field modulated microwave absorption spectroscopy (MFMMS) of lithiated FeSe hydroxide at different DC fields. The spectra are shifted vertically for clarity. The flat lines on the high temperature side of the scans indicate that there is no change in the microwave absorption. The two distinct peaks with an onset at 38 K and approximately 35 K indicate the presence of two well defined superconducting phases. The large background around 15 K is attributed to a variety of dissipation mechanisms as found earlier (see main text). (b) shows the chirality characteristic of a superconductor. (c) Hysteresis loop (M vs. H) at 1.8 K, virgin curve to 9 T, down branch to -9 T and up branch to 9 T (see arrows). The line in between the two branches is the paramagnetic fit (see text). (d) M vs. H hysteresis after subtraction of the fitted paramagnetic contribution, this curve resembles the typical shape of superconducting hysteresis curves and by fitting a stretched exponential, $H_{c2}(T)$ for each curve is found. (e) Zero field (red) and field cooled (black) curves were obtained with 30 Oe DC applied field. The separation point of the ZFC-FC curves at 40 K determines the superconducting transition temperature. A change in the slope around 18 K on both branches indicates the possible onset of magnetic order.

The MFMMS spectrum of the LISH at the lowest field (1.5 mT) as a function of temperature shows an abrupt increase at $T_{\mathrm{MFMMS},1}$ = 38 K which is the typical signature of a superconducting transition (Fig. 2).[29] Decreasing the temperature further reveals a strong and broad feature centered around 15 K which is also observed in MFMMS spectra of the non-magnetic "sister" compound KFeSe[36] and further in a variety of cuprates.[37,38] Yazici et al. [36] relate the origin of a similar broad peak to additional dissipation mechanisms like vortex motion and pinning, a Bragg glass-vortex liquid transition or Josephson junctions (weak links) which create additional microwave absorption in the MFMMS.[29] Therefore the broad peak observed in the MFMMS spectra is assigned to a "background" which is not necessarily related to the phase purity and the onset of a magnetic or new superconducting phase. A ferromagnetic transition manifests itself as a dip as opposed to a peak and is difficult to detect due to the background peak.

When the applied magnetic field is increased to 20 mT the background decreases and a second transition around 32 K with an abrupt peak onset at approximately $T_{\mathrm{MFMMS},2} = T_{\mathrm{SC2}} =$ 35 K becomes more pronounced, and is clearly distinct at 30 mT (Fig. 2a). Both peaks shift as a function of field to lower temperatures, as is typical for SC. Both observations together indicate two different SC transitions related to two phases.[28,29] An isothermal, low-field scan at 25 K shows a clockwise chirality which further supports the superconducting nature of the transitions (Fig. 2 (b)).[29]

Standard ZFC-FC magnetometry was performed with 30 Oe applied field using the protocol described above (Fig 2e). The separation of the two magnetization branches at T_t = 40 K defines the SC transition temperature. The ZFC cooled curve saturates at low temperature and it implies full diamagnetism at 2 K. The slight upturn in both the ZFC and FC curves indicates ferromagnetic ordering.

Isothermal magnetization measurements produced hysteresis curves which consist of the superposition of a paramagnetic curve and the hysteresis loop of a conventional superconductor (Fig. 2c). To isolate the superconducting part of the signal a paramagnetic contribution had to be subtracted (Fig. 2d). Simple paramagnetism implies that the magnetization per unit cell n(T) behaves as Brillouin functions using Curie's law[39] with a *g*-factor, g = 2, and momenta J=3/2, S=1/2 and L=1. However, the fitting parameter n(T) is a function of temperature and constant only between 13 and 30 K (Fig. 3b). In this temperature region the paramagnetic contribution of n(13-30K) = 1.8μ_B per unit cell is compatible with the estimation of an upper limit: 2.64μ_B, using bcc iron. The number of Fe atoms is 1.2 per unit cell and a magnetic moment per unit cell for iron in bcc form is 2.2μ_B/Atom$_{Fe}$. Below 13 K n(T) decreases which suggests a change in the total magnetic order at 13 K. Roughly above 30 K n(T) increases with temperature which supports another transition tentatively due to superconductivity setting in at that temperature supported by MFMMS at T_{SC2} = 35 K.

After separating the paramagnetic and superconducting contributions, a lower (upper) critical field H_{c1} (H_{c2}) for each temperature was extracted from the superconducting hysteresis loop. The lower critical field H_{c1} is the point where the magnetization starts to deviate from the linear field dependence from the virgin curve (black curve, inset, Fig. 2c). The upper critical fields at each temperature, H_{c2}(T) were extracted from the SC hysteresis loops by fitting the data with a stretched exponential and by finding the field at which the upper branch decreases to three times the noise level above zero. Below 6 K the magnetic field of 9 T was not enough to close the loops and the upper critical fields were extrapolated.

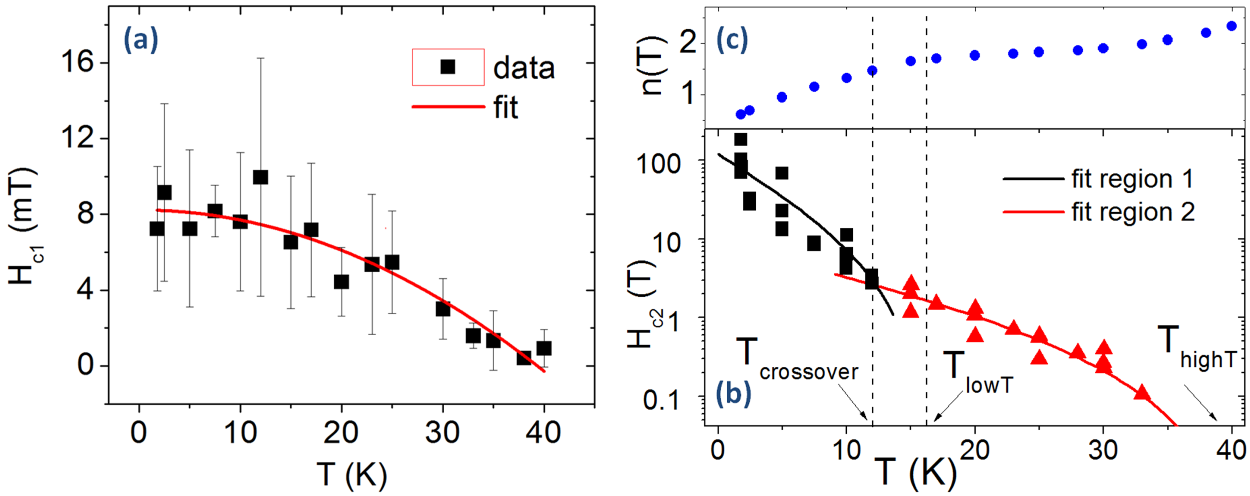

FIG. 3: Lower critical field H_{c1}(T) in (a) and the upper critical fields H_{c2}(T) in (b) as a function of temperature. The upper critical fields are fit with two different curves, each representing a different magnetic phase. In (c) the paramagnetic fit parameter n(T) representing the magnetization per unit cell is plotted as a function of temperature. A change in slope **occurs** around 33 K, **and at T_{lowT}, close to $T_{crossover}$** = **T_M =12 K, likely the crossover** between the two magnetic phases.

The zero-temperature upper and lower critical fields $H_{c1,2}$ (T=0) can usually be obtained from an extrapolation to T=0 of $H_{c1,2}$ (T) with the following expressions.[40,41,42]

$$H_{c1}(T) = H_{c1}(0K)\left[1-\left(\frac{T}{T_c}\right)^2\right] \tag{1}$$

$$H_{c2}(T) = H_{c2}\,(0K)\left[\frac{1-\left(\frac{T}{T_c}\right)^2}{1+\left(\frac{T}{T_c}\right)^2}\right] \tag{2}$$

The lower critical field is therefore determined to $H_{c1}(0K) = 8.3 \pm 0.4\, mT$ with a transition temperature of 39.3 ± 1.3 K. The error bars in figure 3(a) are the standard deviations from approximately 10 different experimental measurements of 5 samples of the lower critical field at each temperature. MgB_2 has a comparable lower critical field.[43-45]

The temperature dependence of H_{c2}(T) has two regimes which we fit independently with the model (2). The high temperature, low critical field regime has a critical field of $H_{c2}^{I}(0\mathrm{K}) = 9$ T and transition temperature of T_{highT} = 41 K, while the low temperature, high critical field regime **is fit with** a critical field of $H_{c2}^{II}(0\mathrm{K}) = 120$ T and a transition temperature of $\mathbf{T_{lowT}}$ = 17 K (Fig. 3 (b)). **An experimentally observable magnetic crossover can be seen in figure 3 b five K lower**, at T_M = 12 K at which the H_{c2}(T) curvature changes similar to low temperature magnetic superconductors and to **several related theoretical publications, which implies a change in magnetic ordering at this observed crossover temperature, $\mathbf{T_M}$ = 12 K**.[10,46,47]

$H_{c2}^{I}(0\mathrm{K}) = 9$ T, derived from the high temperature region, is comparable to the upper critical field at zero temperature obtained from the experimental data in this regime with the Werthamer-Helfand Hohenberg (WHH) aproximation.[48] Earlier published values for LISH are in the same order of magnitude as $H_{c2}^{II}(0\mathrm{K}) = 120$ T.[49,50]

The superconducting coherence lengths $\xi_{I,\,II}$ (T=0) were extracted using the Ginzburg Landau equations[51,52] with $\Phi_0 = 2\cdot10^{-7}\mathrm{Gcm}^2$

$$\xi\,(T{=}0) = \left(\frac{\Phi_0}{2\pi\mu_0 H_{c2,T=0}}\right)^{\frac{1}{2}}. \qquad (3)$$

ξ_I = 5.95 nm and ξ_{II} = 1.63 nm are at least 15 times smaller than the structural characteristic length (91 ± 7 nm) obtained from XRD as described previously. Since $H_{c2}^{I}(0\mathrm{K}) = 9$ T is the smaller of the two upper critical fields, ξ_I calculated using $H_{c2}^{I}(0\mathrm{K})$ represents an upper limit for the SC coherence length. This implies that the structural information obtained with XRD is an average over a length scale which is much larger (~15 times) than the longest superconducting length scale. Therefore the material appears structurally uniform while it is inhomogeneous on the length scales relevant to superconductivity, as shown by the two MFMMS peaks at $T_{\mathrm{SC2}} = 35$ K and $T_{\mathrm{MFMMS,1}} = 38$ K. It is noteworthy that transport and susceptibility measurements are intrinsically unable to detect the various phases in the type of sample presented here.

V. CONCLUSION

The highest transition temperature determined by MFMMS, $T_{\mathrm{MFMMS,1}} = 38$ K, is in agreement with the transition temperature determined from the ZFC-FC curves and the analysis of the upper critical fields. This implies a superconducting transition of $[(\mathrm{Li}_{1-x}\mathrm{Fe}_x)\mathrm{OH}]\mathrm{FeSe}$ (LISH) at $T_{\mathrm{SC1}} = 40 \pm 2$ K in agreement with the literature. **The upper critical fields suggest a magnetic transition at the crossover temperature $T_{\mathrm{M}} = 12$ K.** The MFMMS data is not conclusive in that temperature range.

Remarkably the upper critical field at zero temperature is enhanced more than one order of magnitude by the magnetic ordering. Enhancements of $H_{c2}(T)$ of smaller magnitudes have been observed previously in antiferromagnetic and ferromagnetic superconductors.[53-55] A recent neutron powder diffraction study[24] of $(^{7}\mathrm{Li}_{0.82}\mathrm{Fe}_{0.18}\mathrm{OD})\mathrm{FeSe}$ found no evidence for an antiferromagnetic ordering although ferromagnetic order could not be excluded, while the theoretical results of Liu et al show the coexistence of ferromagnetism and superconductivity.[56] This together with our experiment suggests that the magnetic order below **$T_{\mathrm{M}} = 12$ K** in LISH is ferromagnetic.

In summary, we found two clear and distinct transition temperatures within structurally homogeneous LISH. This has implications for new unconventional doped superconductors which are inhomogeneous on sufficiently small length scales. In-depth analysis of the magnetometry data implies that the superconducting phase coexists with a **magnetic order,**

below T_M = 12 K. This magnetic order is consistent with ferromagnetism and greatly enhances the critical field of the superconducting state. Ferromagnetism enhanced critical fields were previously observed in literature in other materials but the enhancement we found in LISH is significantly larger than in any other reported material. This opens the possibility of tuning critical fields in superconductors using functional materials in which superconductivity and ferromagnetism coexist.

ACKNOWLEDGEMENTS

We gratefully acknowledge the financial support by the German Research Foundation (DFG), Grant JO257/7-1. Research at UCSD is supported by an AFOSR grant FA9550-14-1-0202.

REFERENCES

1 H. Schmid, Ferroelectrics, **162**, 317 (1994).

2 J. E. Hirsch, M. B. Maple, and F. Marsiglio, Physica C: Superconductivity and Its Applications **514**, 1 (2015).

3 A. Ohtomo, and H. Y. Hwang, Nature **427**, 6973, 423 (2004)

4 L. Li , C. Richter, J. Mannhart, and R. C. Ashoori, Nat. Phys. **7**, 762 (2011).

5 J. de la Venta, S. Wang, J. G. Ramirez, and I. K. Schuller, Appl. Phys. Lett. **102**, 122404 (2013).

6 R. Chevrel, M. Sergent, and Prigent, J. Solid State Chem. **3**, 515 (1971).

7 B. T. Matthias, M. Marezio, E. Corenzwit, A. S. Cooper, and H. E. Barz, Science **175**, 1465 (1972).

8 Ø. Fischer, A. Treyvaud, R. Chevrel, and M. Sergent, Solid State Commun. 17, 721 (1975)

9 A. Butera, A. Fainstein, E. Winkler, and J. Tallon, Phys. Rev. B **63**, 054442 (2001).

10 H. Eisaki, H. Takagi, R. J. Cava, B. Batlogg, J. J. Krajewski, W. F. Peck, Jr., K. Mizuhashi, J. O. Lee, and S. Uchida, Phys. Rev. B **50**, 647 (1994).

11 E.-M. Anton, S. Granville, A. Engel, S. V. Chong, M. Governale, U. Zulicke, A. G. Moghaddam, H. J. Trodahl, F. Natali, S. Vezian, and B. J. Ruck, Phys. Rev. B **94**, 024106 (2016).

12 H. Homma, C. S. L. Chun, G.-G. Zheng, and I. K. Schuller, Phys. Rev. **B** 33, 3562 (1986).

13 I. K. Schuller and H. Homma, MRS Bulletin **12**, 18 (1987).

14 H. Kobayashi , A. Kobayashi, and P. Cassoux, Chem. Soc. Rev. **29**, 325 (2000).

15 E. Coronado, C. Martí-Gastaldo, E. Navarro-Moratalla, A. Ribera, S. J. Blundell, and P. J. Baker, Nat. Chem. **2**, 1031 (2010).

16 A. J. Drew, C. Niedermayer, P. J. Baker, F. L. Pratt, S. J. Blundell, T. Lancaster, R. H. Liu, G. Wu, X. H. Chen, I. Watanabe, V. K. Malik, A. Dubroka, M. Rössle, K. W. Kim, C. Baines, and C. Bernhard, Nat. Mater. **8**, 310 (2009).

17 E. Slooten, T. Naka, A. Gasparini, Y. K. Huang, and A. de Visser, Phys. Rev. Lett. **103**, 097003 (2009).

18 C. T. Wolowits, B. D. White, and M. B. Maple, Physica C **514**, 113 (2015).

19 U. Pachmayr, F. Nitsche, H. Luetkens, S. Kamusella, F. Brückner, R. Sarkar, H.-H. Klauss, and D. Johrendt, Angew. Chem. Int. Edit. **54**, 293 (2015).

20 X. F. Lu, N. Z. Wang, H. Wu, Y. P. Wu, D. Zhao, X. Z. Zeng, X. G. Luo, T. Wu, W. Bao, G. H. Zhang, F. Q. Huang, Q. Z. Huang, and X. H. Chen, Nat. Mater. **14**, 325 (2015).

21 U. Pachmayr and D. Johrendt, Chem. Commun. **51**, 4689 (2015).

22 Y. P. Wu, D. Zhao, X. R. Lian, X. F. Lu, N. Z. Wang, X. G. Luo, X. H. Chen, and T. Wu, Phys. Rev. B **91**, 125107 (2015).

23 F. Nejadsattari and Z. M. Stadnik, J. Alloys Compd. 652, 470 (2015).

24 J. W. Lynn, X. Zhou, C. K. H. Borg, S. R. Saha, J. Paglione, and E. E. Rodriguez, Phys. Rev. B **92**, 060510(R) (2015).

25 H. Sun, D. N. Woodruff, S. J. Cassidy, G. M. Allcroft, S. J. Sedlmaier, A. L. Thompson, P. A. Bingham, S. D. Forder, S. Cartenet, N. Mary, S. Ramos, F. R. Foronda, B. H. Williams, X. Li, S. J. Blundell, and S. J. Clarke, Inorg. Chem. **54**, 1958 (2015).

26 X. F. Lu, N. Z. Wang, G. H. Zhang, X. G. Luo, Z. M. Ma, B. Lei, F. Q. Huang, X. H. Chen, Phys. Rev. B **89**, 020507 (2014).

27 S. H. Glarum, J. H. Marshall, and L. F. Schneemeyer, Phys. Rev. B **37**, 7491 (1988).

28 S. Guenon, J.G. Ramirez, A. C. Basaran, J. Wampler, M. Thiemens, S. Taylor, and I. K. Schuller, Sci. Rep. **4**, 7333 (2014).

29 J. G. Ramírez, A. C. Basaran, J. de la Venta, J. Pereiro, and I. K. Schuller, Rep. Prog. Phys. **77**, 093902 (2014).

30 J. Stankowski and B. Czyźak, Appl. Magn. Reson. **2**, 465 (1991).

31 B. F. Kim, J. Bohandy, K. Moorjani and F. J. Adrian, J. Appl. Phys. **63**, 2029 (1988).

32 H. M. Rietfeld, J. Appl. Cryst. **2**, 65 (1969).

33 L. B. McCusker, R. B. Von Dreele, D. E. Cox, D. Louër, and P. Scardi, J. Appl. Cryst. **32**, 36 (1999).

34 A. Coelho, TOPAS-Academic, Version 4.1, Coelho Software, Brisbane (2007).

35 M. A. Beno, L. Soderholm, D. W. Capone II, D. G. Hinks, J. D. Jorgensen, J. D. Grace, I. K. Schuller, C. U. Segre, and K. Zhang, Appl. Phys. Lett. **51,** 57 (1987). (YBCO structure)

36 D. Yazici, A. C Basaran, J. G. Ramírez, I. K. Schuller, and M. B. Maple, Supercond. Sci. Technol. **29**, 085015 (2016).

37 J. Bohandy, F. J. Adrian, B. F. Kim, K. Moorjani, R. D. Shull, L. J. Swartzendrµer, L. H. Bennett, and J. S. Wallace, J. Supercond. **1**, 191 (1988).

38 K. Moorjani, J. Bohandy, F. J. Adrian, B. F. Kim, R. D. Shull, C. K. Chiang, L. J. Swartzendruber, and L. H. Bennett, Phys. Rev. B **36**, 4036 (1987).

39 N. W. Ashcroft, and N. D. Mermin, *Solid state physics* (Holt, Rinehart and Winston, New York, 1976), p. 655.

(1996).

40 J. W. Rohlf, *Modern Physics from a to Z* (Wiley, New York, 1994), p. 646.

(1996).

41 X. Zhu, H. Yang, L. Fang, G. Mu, and H.-H. Wen, Supercond. Sci. Technol. **21,** 105001 (2008).

42 L. Fang, Y. Wang, P. Y. Zou, L. Tang, Z. Xu, H. Chen, C. Dong, L. Shan, and H. H. Wen, Phys. Rev. B **72,** 014534 (2005).

43 A. D. Caplin, Y. Bugoslavsky, L. F. Cohen, L. Cowey, J. Driscoll, J. Moore, and G. K. Perkins, Supercond. Sci. Technol. **16**, 176 (2002).

44 K.-H. Müller, G. Fuchs, H. Handstein, K. Nenkov, V. N. Narozhnyi, and D. Eckert, J. Alloys Compd. **322,** L10 (2001).

45 S. L. Bud'ko, C. Petrovic, G. Lapertot, C. E. Cunningham, P. C. Canfield, M.-H. Jung, and A. H. Lacerda, Phys. Rev. B **63**, 220503 (2001).

46 E. I. Blount, and C. M. Varma, Phys. Rev. Let. **42**, 1079 (1979)

47 O. Fischer, *Ternary Superconductors,* G. K. Shenoy, B. D. Dunlap, and F. Y. Fradin, (Elsevier North Holland, Inc., New York, 1981), p. 303.

48 N. R. Werthamer, E. Helfand, and P. C. Hohenberg, Phys. Rev. **147**, 295 (1966).

49 C. Wang, X. Yi, Y. Qiu, Q. Tang, X. Zhang, Y. Luo, and B. Yu, Supercond. Sci. Technol. **29,** 055003 (2016).

50 Z. Wang, J. Yuan, J. Wosnitza1, H. Zhou, Y. Huang, K. Jin, F. Zhou, X. Dong, and Z. Zhao, J. Phys. Condens. Matter **29**, 025701 (2017)

51 V. L. Ginzburg, L. D. Landau Zh. Eksp. Teor. Fiz. **20**, 1064 (1950)

52 C. S. Yadav and P. L. Paulose, New J. Phys. **11**, 103046 (2009).

53 H. C. Hamaker, L. D. Woolf, H. B. MacKay, Z. Fisk, and M. B. Maple, Solid State Commun **32**, 289 (1979)

54 Ø. Fischer, M. Ishikawa, M. Pelizzone, and A. Treyvaud, J Phys Colloques **40**, 89 (1979)

55 K. Machida, K. Nokura, and T. Matsubara, Phys Rev B 22, 2307 (1980)

56 D.-Y. Liu, Z. Sun, and L.-J. Zou, New J. Phys. **19**, 023028 (2017)